V European Conference on Computational Fluid Dynamics
ECCOMAS CFD 2010
J. C. F. Pereira and A. Sequeira (Eds)
Lisbon, Portugal,14-17 June 2010

ON DRAG COMPUTATIONS OF ROUGH SURFACES: MODELING, SIMULATIONS AND MODEL REDUCTION BY APPLYING HOMOGENIZATION

E. Friedmann* **and T. Richter***

*Department of Applied Mathematics,
Im Neuenheimer Feld 293, D-69120 Heidelberg
e-mail: {friedmann, thomas.richter}@iwr.uni-heidelberg.de

Key words: Navier-Stokes equations, homogenization, direct simulations, boundary conditions, drag reduction, riblets

Abstract. *We present studies on turbulent flow over rough surfaces such as shark skin, which have a drag reducing effect known as shark-skin effect. Simulations of turbulent flow over very small microstructures are challenging, especially if we are interested in a boundary functional like the skin friction. A suitable mathematical model can be formulated only in the viscous sublayer of the turbulent overflow, where the flow can be described by the Navier-Stokes equations. The calculations of the drag can be simplified by using homogenization but the obtained effective model is valid for vanishing microstructures. For applications we consider microstructures with a fixed height and gain for information about the drag compared to a smooth surface. For this direct simulations are performed via stabilized finite elements. We will discuss some numerical and theoretical issues which come along with the simulations of a cutout model, which is a finite part of the viscous sublayer, instead of considering the total turbulent overflow, and how the model can be improved to obtain more realistic information about the drag performing moderate simulations.*

1 INTRODUCTION

In this work we present a model of turbulent flow over rough surfaces in order to analyze the effect of different roughness on the drag force. The microstructures considered are the ones observed on the skin of fast and low swimming sharks. They are very small (0.01-0.2mm) and we assume a periodically distribution. The flow around sharks is turbulent (Re=$10^6 - 10^7$) and following the theory of Prandtl and Schlichting (see [12]) a full turbulent boundary layer is developed which can be divided into sublayers: the viscous buffer, logarithmic and outer sublayer. We restrict our model only to the viscous sublayer, i.e. a cutout of the turbulent overflow with introduced boundaries on which we have to impose the correct in-, outflow and boundary conditions. In this way we model turbulent flow using only the well developed analysis concerning viscous flow and we do not have to utilize some conceptual analysis which has to be connected with the complexity and intractability of the mathematical description of turbulent flow. We will examine how the linear profile is disturbed by different microstructures and how these disturbances affect the drag force.

2 The model of the viscous sublayer

The viscous sublayer is a thin layer of fluid (thickness: $0 < y^+ \leq 5$, where y^+ is the dimensionless characteristic wall coordinate), which is slowed down near the wall through friction forces so that the velocity profile shows values from zero (no-slip boundary condition) to the frictionless external velocity U_∞ of the flow. Here the flow can be well described by the stationary incompressible Navier-Stokes equation with a linear velocity profile, the Couette profile. We model a cutout of the viscous boundary layer, i.e. a straight three-dimensional channel with a rough bottom (see figure 1). The main flow direction is chosen to be parallel to the x_1-axis and is called the longitudinal flow. The way to model the Couette flow in the viscous sublayer of a turbulent flow is to prescribe the velocity on the upper boundary with $U = (U_1, U_2, 0)$ and no-slip condition on the rough surface. U_1 is the velocity of the main flow and U_2 is the velocity of the so-called cross flow which is induced by the vortices in the turbulent flow above.

The so-called canonical cell of roughness is denoted by $Z = (0, b_1) \times (0, b_2) \times (0, b_3)$ and is plotted in figure 2. The rough boundary is denoted by $\gamma(y_1, y_2)$, where $y_1, y_2 \in (0, b_1) \times (0, b_2)$ are the macroscopic variables. The fluid part of this cell is denoted by $Y = \{y \in Z |$ $b_3 > y_3 > \max\{0, \gamma(y_1, y_2)\}\}$. The layer of roughness is $\mathcal{R}^\varepsilon = (\cup\varepsilon(Y + (k_1, k_2, -b_3))) \cap ((0, L_1) \times (0, L_2) \times (-\varepsilon b_3, 0))$. The rough boundary $\mathcal{B}^\varepsilon = \varepsilon(\cup\gamma + (k_1, k_2, -b_3))$ consists of a large number of periodically distributed humps of characteristic length ε but variable height εh with $h \in [0, 1]$. The region above the layer of roughness is denoted by $P = (0, L_1) \times (0, L_2) \times (0, L_3)$. The interface which separates the smooth domain P from the layer of roughness is denoted by $\Sigma = (0, L_1) \times (0, L_2) \times (0)$. It is the artificial smooth interface which will be introduced in the homogenization process. Thus, the region where

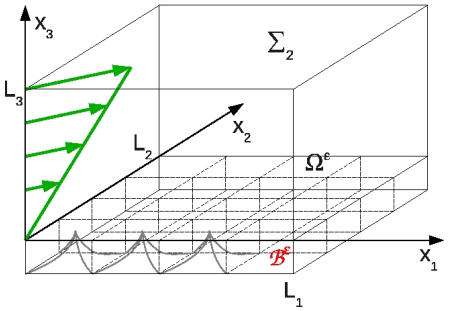

Figure 1: *The three-dimensional viscous sublayer on a rough surface.*

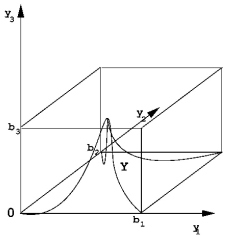

Figure 2: *The three-dimensional canonical cell of roughness.*

the fluid flows is $\Omega^\varepsilon = P \cup \Sigma \cup \mathcal{R}^\varepsilon$ (see figure 1). With Σ_2 we denote the upper interface $(0, L_1) \times (0, L_2) \times \{L_3\}$, where the velocity is prescribed.

The steady state incompressible Navier-Stokes equation for the three-dimensional viscous sublayer reads as follows:

$$\begin{cases} -\nu\Delta v^\varepsilon + (v^\varepsilon\nabla)v^\varepsilon + \nabla p^\varepsilon &= 0, \text{ in } \Omega^\varepsilon \\ \operatorname{div} v^\varepsilon &= 0, \text{ in } \Omega^\varepsilon \\ v^\varepsilon &= 0, \text{ on } \mathcal{B}^\varepsilon \\ v^\varepsilon &= U, \text{ on } \Sigma \\ \{v^\varepsilon, p^\varepsilon\} &- (x_1, x_2) \text{ periodic.} \end{cases} \tag{1}$$

The data for our model are: the viscosity of water, $\nu_{water} = 1.01 \times 10^{-6} m^2/s$, the size of the viscous sublayer, $\delta \sim \sqrt{\nu} = 10^{-3}$ m and the shear velocity, $|U| = \sqrt{\frac{\tau}{\rho}} = 10^{-3}$. In the viscous sublayer we have a low Reynolds number (Re ≈ 1). We assume that the boundary layer thickness and the velocity component parallel to the surface are independent from (x_1, x_2), they do not vary along the wall. This restriction is natural in our case where we consider only a very small part of the total surface.

The drag which is the force that resists the movement of a solid object through a fluid is made up of friction forces, which act in the direction parallel to the surface, plus pressure forces, which act in the direction perpendicular to the surface. In our case the surface of the object is the oscillating boundary $\mathcal{B}^\varepsilon$ with normal n. Then, the drag is given by:

$$D = \mathcal{F}_t^\varepsilon = \mathcal{F}_{\text{fric}} + \mathcal{F}_{\text{pres}}. \tag{2}$$

In the three-dimensional case the drag force on the rough boundary is a two-dimensional vector:

$$\begin{aligned} \left(\mathcal{F}_{\text{t}}^\varepsilon\right)_1 &= \frac{1}{L_1 L_2} \int_{\mathcal{B}^\varepsilon} \nu\sigma n e_1 dx_1 dx_2 \\ &= \frac{\nu}{L_1 L_2} \int_{\mathcal{B}^\varepsilon} \Big(2\frac{\partial v_1^\varepsilon}{\partial x_1} - p\Big) n_1 + \Big(\frac{\partial v_1^\varepsilon}{\partial x_2} + \frac{\partial v_2^\varepsilon}{\partial x_1}\Big) n_2 + \Big(\frac{\partial v_1^\varepsilon}{\partial x_3} + \frac{\partial v_3^\varepsilon}{\partial x_1}\Big) n_3, \end{aligned} \tag{3}$$

where $\sigma_{ij} = \frac{1}{2}(\frac{\partial u_i}{\partial x_j} + \frac{\partial u_j}{\partial x_i}) - p\delta_{ij}$ is the total stress tensor, consisting of the viscous shear stress, due to viscous forces in the fluid, and of the pressure p, and

$$\begin{aligned} \left(\mathcal{F}_{\mathrm{t}}^{\varepsilon}\right)_2 &= \frac{1}{L_1 L_2} \int_{\mathcal{B}^{\varepsilon}} \nu \sigma n e_2 dx_1 dx_2 \\ &= \frac{\nu}{L_1 L_2} \int_{\mathcal{B}^{\varepsilon}} \Big(\frac{\partial v_2^{\varepsilon}}{\partial x_1} + \frac{\partial v_1^{\varepsilon}}{\partial x_2}\Big) n_1 + \Big(2\frac{\partial v_2^{\varepsilon}}{\partial x_2} - p\Big) n_2 + \Big(\frac{\partial v_2^{\varepsilon}}{\partial x_3} + \frac{\partial v_3^{\varepsilon}}{\partial x_2}\Big) n_3. \end{aligned} \tag{4}$$

The so-called oscillating drag force $\mathcal{F}_{\mathrm{t}}^{\varepsilon}$ can only be evaluated using costly direct simulations of (1). In this paper we will consider different models with different boundary conditions and will present a model with minimum calculation costs for the drag.

In [6] and [11] this oscillating drag force is replaced by the so-called effective drag force, where the drag is evaluated at the artificial smooth interface Σ using the smooth solution $u^{\mathrm{eff}}, p^{\mathrm{eff}}$ gained in the homogenization process. This so-called effective solution can be calculated analytically. It is the Couette profile given through a different boundary condition on Σ, the Navier slip condition. Inserting $u^{\mathrm{eff}}, p^{\mathrm{eff}}$ in (3), (4) one obtains the following formula

$$\mathcal{F}_t^{\mathrm{eff}} = \frac{\nu}{2} \frac{U}{L_3 - \varepsilon M}, \tag{5}$$

which depends only on the Navier matrix, to be calculated in an auxiliary problem. This auxiliary problem is here of boundary layer type in a semi-infinite rough domain. The equations which have to be solved in this auxiliary problem are the Stokes equations with a jump in the gradient of the velocity on the smooth boundary. In this approximation of the drag the pressure drag disappears because the normal to Σ is the e_3-vector. This approximation holds for small microstructures ($\varepsilon \to 0$). Jäger and Mikelić showed in [11] that the error approximation for the drag is of order $O(\varepsilon^2)$. We are interested in microstructures with a fixed height, i.e. with a fixed ε ($h = \frac{\varepsilon}{2}$), and will analyze in future work how we can do drag predictions for different microstructures using the effective drag force which would minimize the effort for the drag computations.

3 Direct Simulations

Jäger and Mikelić showed in [11] the existence of a solution $\{v^{\varepsilon}, p^{\varepsilon}\} \in H^2(\Omega^{\varepsilon}) \times H^1(\Omega^{\varepsilon})$ of (1) if $|U|\delta < 2\nu$. Numerical simulations for (1) are very difficult especially for the three-dimensional flow problem with very small microstructures. To capture the microstructures with a sufficient accuracy we need a very fine mesh which requires a huge amount of data.

The direct simulations of the oscillating incompressible steady state Navier-Stokes equation (1) were performed using one of the powerful codes developed in the numerical group of R. Rannacher called Gascoigne [9]. We used a finite element discretization with piecewise quadratic polynomials for velocity and pressure to approximate the equations. To cope with the lacking discrete inf-sup condition of the equal order spaces stabilization based on local projections (LPS) [3] is utilized. A key in these direct simulations is the

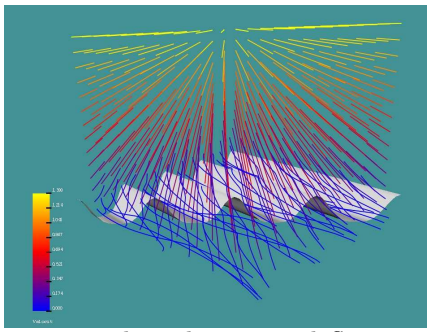

Figure 3: *Three-dimensional flow in the viscous sublayer over riblets.*

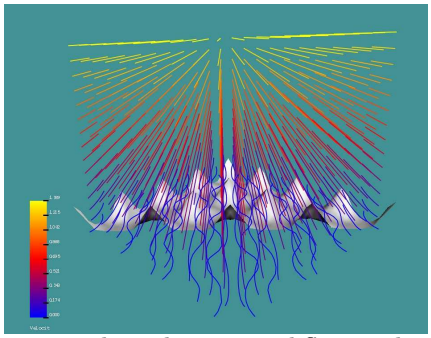

Figure 4: *Three-dimensional flow in the viscous sublayer over a thorn-like structure.*

approximation of the rough boundary by isoparametric finite elements to have an accurate evaluation of the drag which is a boundary functional. Together with these isoparametric finite elements local mesh adaptation (see [2] is used for a higher order representation of the boundary. Due to the low Reynolds number we can directly solve the nonlinear equations (1) with a Newton method. The arising linear systems are solved with a generalized minimal residual method (GMRES) iteration preconditioned by the h-multigrid method. Details on the numerical methods for solving the Navier-Stokes equations are given in [5] and more details on the direct simulation of flow over a shark skin are given in [8].

We will calculate the two components of the drag: the drag in the longitudinal direction which is of main interest (denoted here by $(\mathcal{F}_{\mathrm{t}}^{\varepsilon})_1$ or by drag - x_1 in the tables) and the drag in the cross flow direction (denoted here by $(\mathcal{F}_{\mathrm{t}}^{\varepsilon})_2$ or by drag - x_2 in the tables). The values were obtained after a transformation of the boundary integral into a domain integral to achieve a more accurate evaluation. We also separately calculate the two components of the total drag, the friction- and the pressure-term, in form of a boundary integral.

3.1 Model A

Our first three-dimensional calculations (see figure 3), which we name Model A, have been performed on a $(1.2 \times 1.2 \times 1)$ channel with riblets given by the following shape function: $\gamma(x_1, x_2) = 0.15a(x_2)^2 - 0.15$, where $a(x_2) = 0.5 + 0.5\cos(8/1.2 \cdot x_2\pi)$. The height of the riblets is 0.15 (with respect to 1 as the height of the channel) and the spacing is 0.3 (with respect to 1.2 as the width of the channel). This kind of geometry was chosen after solving a shape optimization problem (see [6]). In Model A we consider the following boundary conditions: no-slip condition on the rough surface $\mathcal{B}^{\varepsilon}$, overflow $U = (U_1, U_2, 0)$ on Σ_2 and a free in- and outflow on the wedge-faces of the channel. The results are listed in table 1.

Under the same flow conditions we calculated the drag for a thorn-like three-dimensional structure (see figure 4) which is given by the following shape function: $\gamma(x_1, x_2) =$

Table 1: The drag and its components for riblets over a channel of length 1.2 × 1.2

N	drag-x_1	drag-x_2	fric-x_1	press-x_1	fric-x_2	press - x_2
1657	1.624	1.666	2.454	0	2.642	1.529
6235	1.616	1.653	2.073	0	1.491	1.161
24093	1.616	1.652	1.829	0	0.807	1.173
94623	1.616	1.654	1.720	0	0.619	1.159
374945	1.617	1.654	1.606	0	0.489	1.123

Table 2: The drag and its components for a thorn-like structure over a channel of length 1.2 × 1.2

N	drag-x_1	drag-x_2	fric-x_1	press-x_1	fric-x_2	press - x_2
1657	1.5984	1.5984	2.5524	0.2713	2.5524	0.2713
6235	1.5658	1.5658	2.0436	0.7178	2.0436	0.7178
24093	1.5622	1.5622	1.6600	0.7524	1.6600	0.7524
94623	1.5644	1.5644	1.2911	0.6482	1.2911	0.6482
374945	1.5650	1.5650	1.1339	0.6024	1.1339	0.6024

$0.15a(x_1)^2a(x_2)^2 - 0.15$ with $a(x_i) = 0.5 + 0.5\cos(8/1.2 \cdot x_i\pi)$ for $i = 1, 2$. The results are listed in table 2.

In table 1 and 2 we see that the values for the total drag (drag-x_i, $i = 1, 2$) converge much better than the values for the two components for the drag (fric-x_i, press-x_i, $i = 1, 2$). This is due to the special evaluation of the drag as a domain integral opposed to the evaluation using boundary integrals for the two components. In the case of riblets the drag is much more reduced in the longitudinal direction which indicates that the riblets must be used always in the main flow direction (along the streamlines). The values for the three-dimensional thorn-like structure are symmetric. For this model the drag is smaller although figure 3 demonstrates the drag reducing mechanism of riblets: Firstly the cross flow and consequently also the magnitude of turbulence is dampened by the riblets and secondly the flow is directed into the main flow direction. Due to the geometry (the thorn-like structure yields a larger computational volume) we have a different amount of in- and outflow if we consider free-stream boundary conditions. Thus Model A does not describe the same flow situation for the two geometries.

3.2 Model B

In our second model the channel is longer: the size is 2.4 × 2.4 × 1. Here we impose Dirichlet in- and outflow conditions for the velocity: $v = 0$ for $x_3 < 0.15$ and $v = (1, 1, 0) \cdot (x_3 - 0.15)/0.85$. This is a Couette profile with $v = 1$ on the upper boundary and $v = 0$ at $x_3 = 0.15$, the position directly above the microstructures. To avoid disturbances induced from these enforced in- and outflow conditions we have enlarged the domain, we however still evaluate the drag forces only on a section of length (0.6 × 0.6) at

Table 3: The drag and its components for a thorn-like structure over a channel of length 2.4×2.4 with different outflow conditions

boundary conditions	drag	fric	press
Dirichlet (in- & outflow)	0.285	0.178	0.104
Dirichlet inflow & free outflow	0.319	0.198	0.116

the position $[1.2..1.8] \times [1.2..1.8]$ where the flow is more adjusted to the different shapes of microstructures.

We further compare the results with a third configuration, a mixture of Dirichlet inflow with free outflow conditions. The results for both cases are given in table 3 where the numbers are obtained at the finest computational mesh and represent the drag in the main flow direction.

Normalizing the obtained numbers for the drag from Model A and B we obtain 1.0868 for free in- and outflow, 0.8861 for Dirichlet in- and free outflow and 0.7917 for Dirichlet in- and outflow. The values differ quiet much which indicates that we have to be very careful in comparing the drag and in calculating the amount of drag reduction on a cut out model with imposed boundary conditions on the inserted walls.

We also analyze the influence of the channel length on the drag (see table 4).

Table 4: The drag and its components for a thorn-like structure evaluated at different positions

domain	drag	fric.	press.
$0.9 \times 0.9 \times 1$	0.16	0.095	0.03
$1.8 \times 1.8 \times 1$	1.50 ± 0.02	1 ± 0.05	0.515 ± 0.01
$2.7 \times 2.7 \times 1$	4	4.5	0.8

Normalizing the numbers from table 4 we obtain 0.1975, 0.463 and 0.548 for the drag calculated with the same model. Again, the values obtained differ too much from each other, so that we are still far to have an adequate model.

3.3 Model C

In our third model we consider an even longer channel of size $(3.6 \times 3.6 \times 1)$. We use the in- and outflow conditions as proposed in Model B, i.e. Dirichlet boundary condition for in- and outflow and Dirichlet boundary condition for the inflow and free outflow. The drag is evaluated on a small domain $([0..0.6] \times [0..0.6])$ inside the channel at the same position. Results are given in table 5.

Comparing the values from table 3 with table 5 we observe that the values for the model with Dirichlet in- and outflow are comparable. The values from the model with Dirichlet in- and free outflow differ too much. Interesting is the observation that the drag gets smaller for a longer channel.

Table 5: The drag and its components for a thorn-like structure over a channel of length 3.6 × 3.6 with different outflow conditions

boundary conditions	drag	fric	press
Dirichlet (in- & outflow)	0.286	0.175	0.103
Dirichlet inflow & free outflow	0.297	0.181	0.107

Table 6: The drag and its components for a thorn-like structure over a channel of length 3.6 × 3.6 with different outflow conditions evaluated at different positions

evaluation position	boundary condition	drag	fric	press.
[1.2..1.8]x[1.2..1.8]	Dirichlet (in- & outflow)	0.286	0.175	0.103
	Dirichlet inflow & free outflow	0.297	0.181	0.107
[1.8..2.4]x[1.8..2.4]	Dirichlet (in- & outflow)	0.287	0.176	0.104
	Dirichlet inflow & free outflow	0.315	0.193	0.114
[2.4..3.0]x[2.4..3.0]	Dirichlet (in- & outflow)	0.285	0.174	0.103
	Dirichlet inflow & free outflow	0.343	0.210	0.125

In table 6 we consider different evaluation positions for the drag with the two types of boundary conditions.

In this subsection we can conclude that the values for the model with Dirichlet in- and outflow boundary conditions are stable. In the model using free outflow condition we observe large fluctuations in the values for the drag. The closer the evaluation position gets to the free outflow boundary the larger the values of the drag.

3.4 Model D

In our last model we consider a channel of length 3.6 × 3.6 with different Dirichlet conditions for the velocity: $v = 0$ for $x_3 < 0.1$ and $v = (1, 1, 0) \cdot (x_3 - 0.1)/0.9$. The Couette profile is shifted downwards by 0.05 such that the origin of the Couette flow profile is located under the tips of the microstructures. The idea behind this condition is to prescribe the Couette in- and outflow in the same way it is adjusted automatically through the microstructures. This is important if we would like to evaluate the drag in a shorter channel to keep the computation costs lower. This model has also the advantage that it is comparable to the experiments performed at DLR (see [1] and [10]). The drag and its components are evaluated in the domain [2.4..3.0]x[2.4..3.0]. We compare the values for the three different boundary conditions: Dirichlet in- and outflow, Dirichlet in- and free outflow and free in- and outflow (see table 7).

From these calculations we conclude that there is a large variation in the drag values. Prescribing Dirichlet condition for in- and outflow yields the most stable results for the direct simulations of our cutout problem (1).

Table 7: The drag and its components for a thorn-like structure over a channel of length 3.6×3.6 with different outflow conditions

boundary condition	drag	fric	press.
Dirichlet (in- & outflow)	0.361	0.220	0.132
Dirichlet inflow & free outflow	0.379	0.231	0.138
free overflow & no-slip	0.398	0.243	0.146

Table 8: The drag and its components on the two geometries

	drag - x_1	fric - x_1	press. - x_2	drag - x_2	fric - x_2	press. - x_2
thorns	0.361	0.224	0.132	0.361	0.224	0.132
riblets	0.419	0.411	0	0.471	0.123	0.327

3.5 Proposed model for the comparison of the drag between different geometries

Summarizing former tests and observations allows to define the new model: The channel is $(3.6 \times 3.6 \times 1)$, the Couette profile is prescribed in the channel by the no-slip condition on the rough surface and the stream velocity on the upper boundary, the in- and outflow is prescribed by a Couette flow with the origin at $x_3 = 0.1$, $(v = (1, 0, 1) \cdot (x_3 - 0.1)/0.9$ for $0.1 < x_3 \leq 1)$ and $v = 0$ for $x_3 < 0.1$. Both geometries (riblets and thorn-like structures) start with a valley in x_2 - direction (cross flow). The drag is evaluated at the position $[2.4..3] \times [2.4..3]$ inside the channel. The results are presented in table 8.

4 Discussions

For the thorn-like structure the new model produces a lower drag than the first one (Model A). The normalized value drops from 1.0868 to 1.00278. Compared with the smooth surface situated at the position $x_3 = 0.15$, which has a drag of 1.1765, we obtain a drag minimization of 15% and compared with a smooth surface at the position $x_3 = 0.1$ we obtain 10% drag reduction. Only by changing our model we doubled the contribution to drag reduction of thorn-like structures compared with a smooth surface situated directly on the top of the microstructures. The interpretation of these numbers and their comparison with experimental results needs some explanations.

Experiments and tests in a wind channel showed a maximum drag reduction of riblets up to 8%. This result could be improved by experiments in an oil channel (see [1]): For longitudinal blade ribs a drag reduction of 10% was obtained. For technological applications a geometry was proposed which showed a drag reduction of 8.2%. These amounts of drag reduction are not comparable with the ones in our simulations. At first, because these amounts of drag reduction were obtained only for higher microstructures which protrude in the buffer layer of the turbulent boundary layer. For the same height of microstructures as considered in our model only a very low reduction in drag is known.

And secondly, in our simulations the amount of drag reduction depends on the position of the smooth surface which was chosen to be at the same position as the artificial smooth surface constructed for the homogenization process as a reference position. In the experiments the viscous sublayer develops automatically over a flat plate or over a rough surface. Whereas in our cut out model for our simulations the thickness of this layer must be prescribed. The exact thickness of the viscous sublayer which develops in the turbulent flow over microstructures is not known.

Jäger and Mikelić showed in [11], that a change of $O(\varepsilon)$ in the position of the artificial smooth surface Σ (where the effective drag is evaluated) implies a change of order $O(\varepsilon^2)$ in the solution. In [11] Σ was situated at $x_3 = 0.3$ (in our notation). In [6] Σ was situated directly on the top of the microstructures, at $x_3 = 0.15$, and in this paper Σ is situated at $x_3 = 0.1$. For the homogenization process it is less important where the artificial smooth surface is located. The position is only important if we compute and compare the drag of two different configurations for a fixed $\varepsilon \neq 0$.

For riblets our calculations did not show the expected effect of drag reduction. In the new model they even resulted in a larger drag than in our Model A. In [6] we obtained 4.5% drag reduction in the main flow direction with model A. With the new model we obtain only 3%. These amounts stay in comparison with a smooth surface situated at $x_3 = 0.15$. If we compare our results with a smooth surface located at $x_3 = 0.1$ we would even now obtain a drag increase of 1% in the main flow direction and of 3.4% in the cross-flow direction. The differences between the values in table 8 are large. The amount of drag reduction for riblets can be increased by considering optimal geometries as described in [6] and [7]. For our tests with direct simulations we used simpler shapes. We can find shapes of riblets and of real three-dimensional microstructures such that the drag for riblets is lower than for the thorns.

The analyzed models of flow over drag reducing rough surfaces in this paper are an indication of the difficulties which arise from modeling. We conclude, that in our case, Dirichlet in- and outflow conditions were the correct boundary conditions for the artificial boundaries of our finite model. Further research showed that periodic boundary conditions will work as well. They were already implemented and tested in Gascoigne. They have the additional advantage that the domain of computations can be reduced heavily to a single cell which contains only a single roughness. The results of this paper will be compared with simulations with periodic boundary conditions and we will evaluate as well the effective drag for our shapes aiming to do drag predictions on a model with minimal effort.

REFERENCES

[1] D.W. Bechert, M. Bruse, and W. Hage, Experiments with three-dimensional riblets as an idealized model of shark skin, *Experiments in Fluids*, **28**:403-412, (2000).

[2] R. Becker, and R. Rannacher, A feed-back approach to error control in finite element methods: Basic analysis and examples,*East-West J. Numer. Math*, **4** (4):237-264, (1996).

[3] R. Becker, and M. Braack, A finite element pressure gradient stabilization for the Stokes equation based on Local Projections, *Calcolo*, **38** (4):173-199, (2001).

[4] R. Becker, and R. Rannacher, An optimal control approach to a posteriori error estimation in finite element methods, *Acta Numerica 2001*, (2001).

[5] M. Braack, T. Richter, Solution of 3D Navier-Stokes benchmark problems with adaptive finite elements, *Computers and Fluids* , **35** (4), p. 372-392, (2006).

[6] E. Friedmann, *Riblets in the viscous sublayer. Optimal Shape Design of Microstructures*, PhD thesis, Ruprecht - Karls - University Heidelberg, (2005).

[7] E. Friedmann, Optimal Shape Design of two-dimensional riblets, *Journal of Mathematical Fluid Mechanics*, Birkh"auser Basel 2008, http://www.springerlink.com/content/k6t5200527l55671.

[8] E. Friedmann, and T. Richter, Optimal microstructures. Drag reducing mechanism of riblets, *Journal of Mathematical Fluid Mechanics*, submitted (2007).

[9] *Gascoigne - The finite element toolkit*, http://www.gascoigne.uni-hd.de.

[10] W. Hage, *Zur Widerstandsverminderung von dreidimensionalen Riblet-Strukturen und anderen Oberflächen*, Mensch & Buch Verlag, (2005).

[11] W. Jäger, and A. Mikelić, Couette flows over a rough boundary and drag reduction, *Communications in Mathematical Physics*, **232**:429-455, (2003).

[12] H. Schlichting, and K. Gersten, *Boundary-Layer Theory*, 8th revised and enlarged edition, Springer-Verlag, (2000).